Science of the Total Environment 872 (2023) 162118

Contents lists available at ScienceDirect

Science of the Total Environment

journal homepage: www.elsevier.com/locate/scitotenv

Differences between VOCs and NOx transport contributions, their impacts on O_3, and implications for O_3 pollution mitigation based on CMAQ simulation over the Yangtze River Delta, China

Yangjun Wang [a,b], Sen Jiang [a,b], Ling Huang [a,b], Guibin Lu [c], Manomaiphiboon Kasemsan [d,e], Elly Arukulem Yaluk [a,b], Hanqing Liu [a,b], Jiaqiang Liao [a,b], Jinting Bian [a,b], Kun Zhang [a,b], Hui Chen [a,b], Li Li [a,b,*]

[a] School of Environmental and Chemical Engineering, Shanghai University, Shanghai 200444, China
[b] Key Laboratory of Organic Compound Pollution Control Engineering (MOE), Shanghai University, Shanghai 200444, China
[c] School of economics, Shanghai University, Shanghai 200444, China
[d] The Joint Graduate School of Energy and Environment, King Mongkut's University of Technology, Thonburi, Bangkok 10140, Thailand
[e] Center of Excellence on Energy Technology and Environment, Ministry of Higher Education, Science, Research and Innovation, Bangkok 10140, Thailand

HIGHLIGHTS

- Simulated VOCs based on chemical transport models were evaluated with observations.
- Source apportionments of VOC_s, NO_x, and O_3 were performed simultaneously.
- NOx and O_3 have stronger long-distance transport ability than VOCs.
- Regional transport ability of NO_x potentially enhances the regional transport of O_3.

GRAPHICAL ABSTRACT

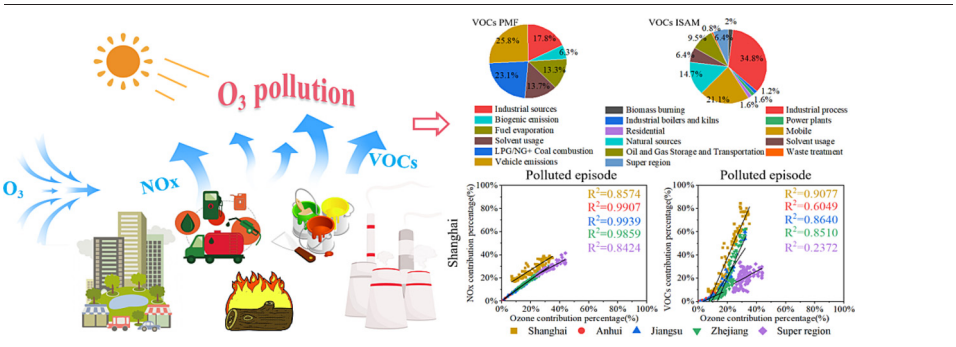

ARTICLE INFO

Editor: Jianmin Chen

Keywords:
Source apportionment
Community Multiscale Air Quality Modeling System (CMAQ)
Volatile organic compounds (VOCs)
Nitrogen oxide (NO_x)
Ozone
Regional transport

ABSTRACT

The relationship between O_3 and its precursors during urban polluted episodes remains unclear. In this study, the simultaneous source apportionment of VOCs, NO_x, and O_3 over the Yangtze River Delta (YRD) region during the O_3 polluted episode on July 24–30, 2018, was performed based on the Integrated Source Apportionment Method (ISAM) embedded in the Community Multiscale Air Quality Modeling System (CMAQ). The results of the ISAM were compared with those of the Brute Force Method (BFM) and Positive Matrix Factorization (PMF). Furthermore, the differences between the transport contributions of VOCs and NO_x, and their impacts on O_3 were analyzed. The results indicate that observations of VOCs species can be well captured by simulated VOCs, and the ISAM has a significant advantage in the source apportionment of VOCs, especially for sources emitting highly reactive species. In the clean and polluted periods, the local contribution percentages of VOCs in urban sites ranged from 60 % to 77 %, much higher than those of NO_x (31 %–43 %) and O_3 (16 %–33 %). NO_x and O_3 have strong transport abilities with high and close contribution percentages, which are highly correlated, mainly because oxygen atoms produced by the photolysis of NO_2 in the aged air mass combined rapidly with O_2 to form O_3 during transport. The VOCs chemical loss caused by the oxidation of OH radicals during transport makes the ability of VOCs for long-distance transport much weaker than that of NO_x. Furthermore, owing to the sufficient aging of VOCs, those contributed by long-distance transport have little effect on O_3. To a certain extent, controlling one's NO_x emissions can help other cities more, while controlling one's VOCs emissions can help itself more. Therefore, it is recommended to attach enough importance to joint prevention and control of NO_x among cities and even long-distance areas to alleviate regional O_3 pollution.

* Corresponding author at: L. Li, School of Environmental and Chemical Engineering, Shanghai University, Shanghai 200444, China.
E-mail address: lily@shu.edu.cn (L. Li).

http://dx.doi.org/10.1016/j.scitotenv.2023.162118
Received 30 December 2022; Received in revised form 4 February 2023; Accepted 4 February 2023
Available online 13 February 2023

1. Introduction

Ground-level ozone (O_3) is a secondary pollutant that adversely affects human health, ecosystems, and climate change (Cohen et al., 2017; Li et al., 2017; Monks et al., 2015; Turner et al., 2016). In recent years, ozone has been one of the primary pollutants hindering air quality compliance in eastern China, particularly in the Yangtze River Delta (YRD) region (Li et al., 2019b; Shu et al., 2019; Wang et al., 2021a). The formation, sources, and reduction of O_3 in densely populated areas of eastern China have become important topics that have attracted increasing attention worldwide (Kang et al., 2022; Li and Fan, 2022; Ren et al., 2022; Wang et al., 2022a). In addition to the downward injection of stratospheric O_3, ground-level O_3 is formed through a series of photochemical reactions involving volatile organic compounds (VOCs) and nitrogen oxides (NO_x) under sunlight (Li et al., 2019a; Lupascu et al., 2022). Understanding the relationship among VOCs, NO_x, and O_3, especially their sources, and the impact of the transport contributions of VOCs and NO_x on O_3 is essential for scientific decision-making on O_3 pollution mitigation.

VOCs are composed of many compounds with widely varying chemical reactivities; therefore, accurately identifying the source of VOCs is difficult. Nevertheless, source apportionment of VOCs is vital for understanding O_3 formation. Receptor models based on observational data are widely used for VOCs source apportionment, such as Principal Component Analysis (PCA), Positive Matrix Factorization (PMF), and Chemical Mass Balance (CMB). The CMB model was used to identify sources of VOCs in a French urban area near industrial sources (Badol et al., 2008). However, CMB is based on the principle of mass conservation; therefore, using this method directly usually introduces large deviations for the source apportionment of VOCs species with high chemical reactivity. In overcoming this limitation, the initial concentrations of VOCs before undergoing chemical reactions were calculated according to the observed VOCs concentrations. Then the source apportionment of VOCs was performed using CMB (Shao et al., 2011), but there were significant uncertainties in the estimation of their initial concentrations. As a simple receptor model, PCA is also a method for VOCs source apportionment, but it often suffers from collinearity problems, which lead to large uncertainties (Wang et al., 2010).

Generally, PMF is the most widely used receptor model for the source apportionment of VOCs (Fan et al., 2021; Su et al., 2019; Yuan et al., 2012). For example, the sources of observed VOCs in the coastal industrial area of Ningbo were studied using PMF, and the results showed that industry-related sources contributed 8.65 %–31.2 % of the VOCs year-round (Yang et al., 2023). In recent years, with the development of VOCs measurement technology, additional compounds with higher time resolution can be measured, and the reliability of PMF VOCs source apportionment results has been improved to a certain extent (Su et al., 2019; Vestenius et al., 2021). However, the determination of the PMF factors is somewhat subjective, and the model does not consider the chemical consumption of VOCs in the atmosphere. Although Wang et al. (2022b) considered the chemical consumption of VOCs by adding chemical kinetics to the PMF model, the revised PMF model still did not involve the series of chemical reactions about the complex chemical relationship among VOCs, NO_x and O_3. In addition, the PMF model cannot identify the contribution of VOCs from emission sources at different geographical locations. Another type of models, the three-dimensional Eulerian chemical transport models (CTMs, e.g. Community Multiscale Air Quality Modeling System [CMAQ] and Comprehensive Air Quality Model with Extensions [CAMx]) are powerful tool to help address these source-receptor questions because these models have a "one-atmosphere" framework, which integrates emission inventories and meteorological fields, and simulates all necessary physical and chemical processes in atmosphere.

The 3D CTM-based Brute Force Method (BFM) can be used to quantitatively identify the source contribution of any pollutant by running the model separately for two simulation scenarios of perturbed and undisturbed emissions and comparing the results of the two simulations. Unfortunately, the sum of all source contributions are not equal to the simulated concentrations in the base case if the model response is nonlinear (Koo et al., 2009; Kwok et al., 2015). The response surface modeling (RSM), extended RSM, and RSM based on polynomial functions can also be applied for analysis of O_3 source contributions (Fang et al., 2020; Xing et al., 2017) but they need the RSM model established based on a large number of BFM scenario simulations. The Ozone Source Apportionment Technique (OSAT) based on CAMx (Wagstrom et al., 2008) (www.camx.com) and the Integrated Source Apportionment Method (ISAM) based on CMAQ (https://cmascenter.org), are expected to be highly efficient and flexible for quantitatively identifying the source contribution from different source categories and regions. Both simulate each tagged species separately through each modeled atmospheric physical and chemical processes, resulting in more accurate quantitative source apportionment than that of BFM (Kwok et al., 2015). In recent years, they have been widely used in scientific research and governmental decision-making (Craig et al., 2020; Hu et al., 2022; Lu et al., 2016; Wang et al., 2022b). Beside O_3, the ISAM also can be used for source apportionment of VOCs (Kwok et al., 2015), but OSAT cannot because of some simplistic assumptions.

The ISAM O_3 approach is a hybrid of source apportionment and source sensitivity in that O_3 production is attributed to precursor sources based on the O_3 formation regime (e.g., for a NO_x-sensitive regime, O_3 is apportioned to participating NO_x emissions) (Kwok et al., 2015). Therefore, the ISAM integrates the chemical relationship among NO_x, VOC, and O_3 in an advanced method. As a result, it has unique advantages for synchronous source apportionment of NO_x, VOC and O_3 and revealing their complex relationship. However, CTMs-based VOCs source apportionment has rarely been conducted in China, and even fewer has been evaluated using VOCs observation data. In addition, the synchronous source apportionment of VOCs, NO_x and O_3 has rarely been performed in China, and the impact of the regional transport of VOCs and NO_x on O_3 remains unclear.

In this study, the CMAQ-based ISAM was used for the simultaneous source apportionment of VOCs, NO_x, and O_3 during severe ozone polluted episodes in the YRD region of China in July 2018. Specifically, the model performance for VOCs was evaluated using VOCs observations. In addition, the source apportionment results of VOCs of the ISAM were compared with those of the BFM and PMF, respectively, and the differences in their performance in quantitatively identifying the sources emitting highly chemically reactive species were discussed. Finally, through the analysis of the source apportionment results of VOCs, NO_x, and O_3, the influences of the transport contribution of VOCs and NO_x on O_3 were revealed, and implications for the emission control strategy for ozone pollution mitigation were provided.

2. Methodology

2.1. Model setup

In this study, CMAQv5.3.2 was used to simulate the chemical and physical processes of the "one-atmosphere" system with the input files of emission inventories and meteorological fields generated by Sparse Matrix Operator Kernel Emissions (SMOKE3.7) and Weather Research and Forecasting (WRFv4.0), respectively. Modeling domains with horizontal resolutions of 36 km, 12 km, and 4 km were simulated with 14 vertical layers (Fig. 1). The third domain was the target domain, covering the entire YRD region composed of Zhejiang, Jiangsu, Anhui and Shanghai. Saprc07tic (Carter, 2010) and aero7i (Lin et al., 2013; Murphy et al., 2017; Pye et al., 2015) were used to simulate gas-phase chemistry mechanisms, aerosol formation, and dynamic processes. The Multi-resolution Emission Inventory of China (http://www.meicmodel.org) of 2017 developed by Tsinghua University was used for the first and second domain simulations. The anthropogenic emissions inventory in the YRD region generated by the SMOKE model was the same as that used in the literature (Wang et al., 2022a). All natural (biogenic) emission inventories were generated using the Model of Emissions of Gases and Aerosols from Nature (MEGANv3.1) (Wang et al., 2021b). The emission inventories and configurations of CMAQ and WRF in this study are the same as those in another study (Wang et al., 2022a).

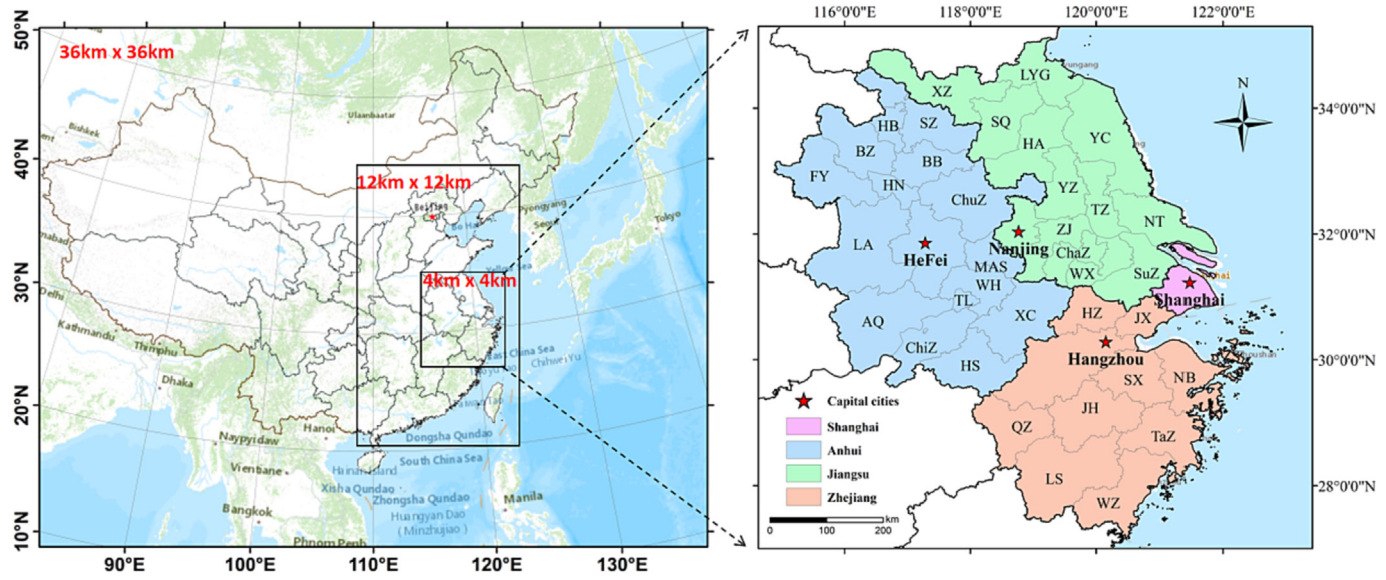

Fig. 1. The domains of the model system used in this study. The 41 cities in YRD are: FY - Fuyang; HZ - Huzhou; HA – Huaian; SuZ – Suzhou (Jiangsu); TaZ – Taizhou; TL – Tongling; AQ - Anqing; BB - Bengbu; BZ-Bozhou; ChaZ - Changzhou; LYG – Lianyungang; LA – Lu'an; NT – Nantong; SZ – Suzhou (Anhui); XZ – Xuzhou; QZ – Quzhou; SX – Shaoxing; HB – Huaibei; HS – Huangshan; JX – Jiaxing; JH – Jinhua; WZ – Wenzhou; WX – Wuxi; ChiZ – Chizhou; LS – Lishui; SQ – Suqian; XC – Xuancheng; YC –Yancheng; NB – Ningbo; WH – Wuhu; ChuZ – Chuzhou; HN – Huainan; MAS – Maanshan; ZJ – Zhenjiang; YZ – Yangzhou and ZS – Zhoushan. Shanghai, Nanjing, Hangzhou and Hefei are the provincial capital cities (red star).

The emission inventory for the target domain comprised ten source categories: biomass burning, industrial processes, industrial boilers and kilns, power plants, residential combustion, mobile source, natural source, solvent usage, oil and gas storage and transportation, and waste treatment (including landfill, incineration, wastewater treatment). The ISAM apportioned the concentrations of pollutants to these ten source categories simultaneously.

The regions involved in the regional source apportionment based on the ISAM include the local city, the province other than the local city, other provinces, and Shanghai. For example, in Hangzhou, where the receptor site is located, the receptor concentration of pollutants is apportioned into four source regions: Hangzhou, Zhejiang province except Hangzhou, Jiangsu province, Anhui province, and Shanghai. The region settings for source apportionment can also be analogized when the receptor site is in another city. Shanghai, Hangzhou, Nanjing, and Hefei are provincial capital cities in Shanghai Municipality, Zhejiang province, Jiangsu province, and Anhui province. To improve the understanding of the sources of VOCs, NO_x and O_3, we selected one urban site and one suburban site of each provincial capital city for a detailed discussion. These typical sites (suburban site, urban site) are in Shanghai (Dianshan Lake; Jing'an), Nanjing (Maigaoqiao; Caochangmen), Hangzhou (Xiasha; Wolong Bridge), and Hefei (Dongpu Reservoir; Mingzhu Square).

Several statistics were used to evaluate the model performance: mean bias (MB), normalized MB (NMB), normalized mean error (NME), root mean square error (RMSE), correlation coefficient (R), and the index of agreement (IOA) (for equations, see Table S2). We conducted a comprehensive evaluation of model performance for the hourly NO_2 and O_3 data from 41 major cities in the YRD region during the simulation time. Moreover, meteorological observation data from four cities' airports (Shanghai: Hongqiao Airport; Hangzhou: Xiaoshan Airport; Nanjing: Lukou Airport; Hefei: Luogang Airport) were used to evaluate the WRF model performance. Overall, the simulation results of the WRF and CMAQ models showed satisfactory agreement with the meteorological observations and pollutant observed concentrations. A detailed evaluation of the model performance is in the Supporting Information.

2.2. Source apportionment

The ISAM is a tagging-based source apportionment method that uses a tracer system to track the sources of pollutants and their precursor species in selected emission categories and geographic areas. Unlike CAMx-OSAT (Li et al., 2019b), which uses two tracers to represent the NO_x and VOC families, ISAM comprises tracers for individual nitrogen and VOC species and considers the maximum incremental reactivity of a single VOC to O_3.

In the CMAQ gas-phase chemistry module, nitrogen and VOC species are updated using a chemical sensitivity approach. For example, explicit VOC tracers are calculated by Eq. (1):

$$\left[VOC_{s,tag}^{new}\right] = \left(I - \frac{\Delta t}{2}J\right)^{-1}\left(I + \frac{\Delta t}{2}J\right)\left[VOC_{s,tag}^{old}\right] \quad (1)$$

Where $VOC_{s,tag}^{new/old}$ is the VOC species for a sector tag before (old) or after (new) the Jacobian calculation, **I** is the identity matrix, **J** is the Jacobian matrix calculated based on the average of bulk concentrations before and after any gas-phase solver. This system is solved by decomposing $\left(I - \frac{\Delta t}{2}J\right)^{-1}\left(I + \frac{\Delta t}{2}J\right)$ into a product of lower and upper triangular matrices, which is known as LU decomposition. The solution is obtained only once for every model synchronization time step Δt (Kwok et al., 2015).

The main way of ozone source apportionment implemented in CMAQ is by using tracers to track individual nitrogen and VOC species. To judge the sensitivity of ozone to VOCs or NO_x in each grid, CMAQ uses the ratio of the H_2O_2 generation rate to the HNO_3 generation rate ($PH_2O_2/PHNO_3$). When $PH_2O_2/PHNO_3 > 0.35$, the grid is identified as VOCs control regime, and when $PH_2O_2/PHNO_3 < 0.35$, it is a NO_x control regime (Sillman, 1999). As we have described, the bulk O_3 concentration in each model grid cell is equal to the sum of the O_3 tracers produced under VOC- or NO_x- sensitive conditions, the calculation could be expressed by Eq. (2):

$$O_{3bulk} = \Sigma_{tag} O_3 V_{tag} + \Sigma_{tag} O_3 N_{tag} \quad (2)$$

Where O_3V_{tag} and O_3N_{tag} are the O_3 attributed to each tagged source in VOC-sensitive and NO_x-sensitive cases, respectively (Kwok et al., 2015). In practice, ozone production and loss processes occur simultaneously, thus, the total PO_3 and DO_3 are calculated to update the O_3 tracer for each time step in the numerical chemistry solver used in the model. The O_3 tracers are updated with the production of intermediate $O_3N_{tag}^{middle}$ for

NO_x-sensitive and $O_3V_{tag}^{middle}$ for VOCs-sensitive using Eqs. (3) and (4), respectively.

$$O_3N_{tag}^{middle} = O_3N_{tag}^{old} + PO_{3bulk} \times \frac{NO_{tag}^{old} + NO_2{}_{tag}^{old}}{\Sigma_{tag}\left(NO_{tag}^{old} + NO_2{}_{tag}^{old}\right)} \quad (3)$$

$$O_3V_{tag}^{middle} = O_3V_{tag}^{old} + PO_{3bulk} \times \frac{\Sigma_s\left(VOC_{s,tag}^{old} \times MIR_s\right)}{\Sigma_{tag}\Sigma_s\left(VOC_{s,tag}^{old} \times MIR_s\right)} \quad (4)$$

In this equation, $O_3N_{tag}^{old}$ and $O_3V_{tag}^{old}$ represent the ozone production under NO_x or VOCs control conditions in the previous time step, respectively. PO_{3bulk} is the chemical production of O_3 per unit time step. $NOC_{x,tag}^{old}$ is the NO_x concentration contribution of the tagged source to the target grid in the previous time step. $VOC_{s,tag}^{old}$ is the contribution of the tagged source to the concentration of individual VOCs in the target grid. Assuming that ozone will be depleted in both regimes for each sector, the distribution of ozone destruction could be expressed by Eq. (5):

$$O_3X_{tag}^{new} = O_3X_{tag}^{middle} + DO_{3bulk} \times \frac{O_3X_{tag}^{middle}}{\Sigma_{tag}\left(O_3N_{tag}^{middle} + O_3V_{tag}^{middle}\right)} \quad (5)$$

where X is either N or V.

Generally, in the CMAQ model, VOCs, NO_x, and O_3 are closely related because of chemical reactions, and the source apportionment results for VOCs, NO_x and O_3 can be obtained simultaneously when the ISAM is implemented. The advantage of this method is that it treats VOCs species separately, unlike the OSAT method of CAMx, which treats VOCs family as one species. Therefore, ISAM can perform source apportionment on VOCs, whereas OSAT cannot.

2.3. Evaluation of VOCs simulation

In this study, the simulation performance of the CMAQ VOCs species was evaluated by comparing the observed VOCs concentration data with the simulated concentrations.

VOCs were measured online from July 22 to 31, 2018 at the Dianshan Lake supersite (120.98°E, 31.09°N), a suburb site of Shanghai. Hundreds of meters from this supersite in the northwest and southwest are Jiangsu and Zhejiang provinces, respectively. The G50 Shanghai-Chongqing Highway is 2.5 km from this supersite in the southeast direction. There were 55 VOCs species—28 species within C7-C12, and 27 species within C2-C6—measured by two online gas chromatographs with flame ionization detector systems. Formaldehyde was also measured by a Hantzsch fluorescence technique (AL4201, Aerolaser GmbH., GER). The atmospheric samples were inhaled directly into the system and was preconcentrated using a low carbon (C2-C6) analyzer and a high carbon (C6-C12) analyzer, respectively. A built-in auto-calibration system, consisting of three permeation tubes (loaded with butane, hexane, and benzene), was used for daily calibration. The VOC standards gas from photochemical assessment monitoring stations was used to perform monthly calibration for this system. Hourly VOCs data were obtained using this system.

VOCs are composed of many compounds. Thus, only a small portion of them can be measured by even the most advanced instruments in the world. Moreover, considering the effectiveness of computing resource utilization, chemical transport models (e.g. CMAQ) cannot and do not necessarily simulate the chemical process of each VOC compound. The number and types of VOCs species contained in the CMAQ model depend on the gas-phase chemical mechanism (SAPRC07i) configured in this study. There are lumped species that represent many organic compounds with similar response rates and mechanisms, such as alkanes and other non-aromatic compounds that react only with OH (ALKn), Alkenes (OLEn), Terpenes (TERP), and Aromatics (AROn). Firstly, according to the User Guide (https://intra.engr.ucr.edu/~Carter/SAPRC), a mapping relationship was established; Next the observed concentration was lumped in terms of this lump rule of the model to obtain the observed concentration of the lumped species. Second, we observed that the lumped species obtained directly from the model still contained VOC species whose concentration was not observed. To improve the accuracy of the simulated concentrations for comparison and verification, we used the Eq. (6) to weigh the simulated concentrations:

$$Conc_{weighted}^{model} = Conc_{lump}^{model} \times \Sigma_{spec}WF_{spec} \quad (6)$$

In this equation $Conc_{weighted}^{model}$ is the weighted concentration of the model lumped species, $Conc_{lump}^{model}$ is the species concentration obtained directly from the model and $\Sigma_{spec}WF_{spec}$ represents the sum of the weighting factors of VOC species with the observed concentrations in the lumped species. Because of the assumption that the weighting factors are fixed and independent of time, the uncertainty of the single VOC species concentration obtained by the model lumped species concentration and weighting factors is greater than the above method. Therefore, we still evaluated according to the weighted lumped species. The species names of model VOCs are listed in Table S7. The lumped relationship between the VOC species and the weighting factors is shown in Table S8.

2.4. Other VOCs source apportionment methods

The source contributions obtained by BFM and EPA PMFv5.0 were compared with those of ISAM in the CMAQ model. For BFM, 11 emission sources of VOCs were zeroed out from the base case to perform 11 simulation scenarios. For PMF, VOCs observations were applied to determine the source contributions of VOCs concentrations at the Dianshan Lake supersite. Additional information on PMF is available in the EPA PMF 5.0 User Guide (Adam, 2007; Norris et al., 2014). Moreover, additional discussions were conducted by comparing the results of the ISAM in this study with the PMF results in other studies over the YRD region.

3. Results and discussion

On July 22, 2018, a famous typhoon (Typhoon Ampil) landed in Shanghai. After the typhoon, the YRD region experienced a severe O_3 polluted episode from July 24–30, 2018. During this period, the O_3–1 h max concentration exceeded the national environmental standard (200 μg/m^3), and the peak value reached 393 μg/m^3. In addition, cities with the highest 8-h average concentrations of ozone (MDA8_O_3) exceeding 160 μg/m^3 accounted for 78.6 % of the YRD region.

3.1. Evaluation of simulated VOCs

Owing to the limitation of VOCs observation data, only the observation data of the Dianshan Lake supersite were used for comparison with the modeled concentrations of VOCs species. From July 22 to 31, the average mixing ratio of total VOCs (TVOC) was 16.61 ± 10.77 ppbv, and the maximum and minimum values were 57.81 and 4.21 ppbv, respectively. The average mixtures of 28 alkanes, 16 aromatic hydrocarbons, 10 alkenes and acetylenes were 9.33 ± 8.05,4.12 ± 3.11,2.15 ± 1.42, and 0.45 ± 0.21 ppbv, respectively. Table S9 summarizes the top 20 VOC species. Among these VOCs, propane had the largest standard deviation, mainly because of the sudden increase in its mixing ratio on July 29, which reached a peak value of 38.87 ppbv.

As shown in Fig. 2, the simulated concentrations of alkanes are in good agreement with the observed concentrations regardless of the daytime or nighttime, except that the observed concentrations of alkanes (mainly propane) were obviously higher than the simulated values in the morning of July 29, which may be due to sudden source emissions (e.g. gas leaks from gas stations) near the Dianshan Lake supersite, which was not considered in the emission inventory. The simulated concentrations of aromatics also agree well with the observed concentrations, except for the overestimates on the morning of July 25 and 31, and an underestimation on the

July 29. The variation pattern of alkenes observed concentration was well captured, although simulations for alkenes did not match observations as well as for aromatics and alkanes. Combined with Fig. S3, it is easy to see that the deviation between the simulation and observation of alkenes is mainly caused by the daytime underestimation of ethylene, which mainly originates from anthropogenic emissions. The comparison of the simulated and observed data for model-explicit species (Fig. S3), shows that several observed high-value periods can be captured well. For example, the concentration peaks of toluene, m-xylene, and o-xylene in the early morning of the 27th can be well simulated, and the peak concentration of ethylene can also be well captured. Another reason for the direct deviation between the simulated and observed concentrations is that the simulated concentrations are based on the average concentration of the grid with an area of 16 km^2 where the Dianshan Lake supersite is located, whereas the observed concentrations are based on this supersite. For more reactive chemical species, the bias owing above reason will generally be larger.

Generally, there are many VOCs compounds in the atmospheric environment, and observing the concentrations of all species is difficult. Similarly, accurately simulating these compounds using a chemical transport model is difficult. Thus, few studies have used the observed concentrations of VOCs species to evaluate the concentrations of VOCs species simulated by chemical transport models, which has outstanding advantages in studying the impact of emissions, meteorological conditions, and chemical processes on air quality. As shown in Table S10, the IOA of alkanes, aromatic hydrocarbons, alkenes, and TVOC were 0.55, 0.74, 0.62, and 0.67, respectively, suggesting a good agreement between the simulations and observations. Overall, the simulation performance of VOCs species shown by the evaluation of this study can be considered good for the further study of source of VOCs for O_3 pollution mitigation.

3.2. Source of VOCs based on the ISAM

Regarding the source contribution of ambient VOCs in the YRD region, industrial processes, natural emissions, and mobile sources were the largest contributors, followed by solvent usage, and oil and gas storage and transportation (Fig. 3). Contributions from natural sources are mainly distributed in densely vegetated areas, whereas their contribution is relatively small in densely populated areas. Industrial sources contributed the most to the ambient VOCs concentration in densely populated areas, followed by mobile sources. Contributions from biomass burning (Fig. 3a) were mainly distributed in Anhui province, a large agricultural province that burns more crop residues than Zhejiang and Jiangsu. Contributions from residential combustion, power plants, industrial boilers and kilns, and waste treatment were relatively low (Fig. S4).

3.3. Comparisons of ISAM and BFM

A comparison of the source contribution results of the ambient VOCs concentrations based on the two methods, that is ISAM and BFM, is shown in Fig. 4. The upper four subfigures show higher contributions than the bottom four subfigures. In the subfigure of the industrial process, more points in Shanghai (blue) fall near the diagonal line than in Nanjing, and more red points (Nanjing) fall below the diagonal line, indicating that the contribution concentrations of VOCs in Nanjing from industrial processes based on the ISAM are greater than those of the BFM for some time. For the contributions from natural sources, most points fall above the diagonal line, implying that the contributions of the BFM from natural sources are larger than those of the ISAM. By contrast, the contributions of the ISAM mobile source were slightly larger than those of the BFM. For oil and gas storage and transportation sources, the source apportionment results based on the two methods were in good agreement, as shown in Fig. 4(d). In general, VOCs emitted from natural sources have higher chemical activity, therefore, the contribution difference between the two methods is relatively larger. This difference also reflects the limitations of the BFM: the stronger the nonlinear relationship, the less reliable the BFM source apportionment results (Kwok et al., 2015).

3.4. Comparisons of ISAM and PMF

Fig. 5 shows the average source contribution percentages of VOCs from July 24 to 31, 2018 at the Dianshan Lake supersite for the PMF method and in its corresponding grid with an area of 16 km^2 for the ISAM. The ISAM results (Fig. 5b) show that the total contribution of combustion sources such as power plants, residences, industrial boilers and kilns is 4.9 %, and the contribution of oil and gas storage and transportation sources is 7.8 %. Based on the ISAM, the sum of the contributions from these sources above was 12.7 %, which can be referred to as the source contributions of coal combustion and oil and gas evaporation. However, the contribution of coal combustion and oil and gas evaporation based on PMF (Fig. 5a) is the sum of the contributions from Liquefied petroleum gas (LPG)/ Natural gas (NG) and coal combustion and fuel evaporation, which is 48.9 %, much higher than the contribution percentage based on ISAM (12.7 %). The main reason for this difference is that PMF, as a source apportionment method based on mathematical statistics, determines its contribution source based on its similarity with the source profile of a certain emission source, suggesting that PMF was more inclined to apportion low-reactivity VOCs to the contributions from the sources (Fig. 5). Isoprene is the dominant VOC species emitted by vegetation. It is short-lived and can only be transported over short distances. The PMF method identifies natural sources based only on isoprene observed at the receptor site, such as the Dianshan Lake supersite, and does not account for the chemical loss of

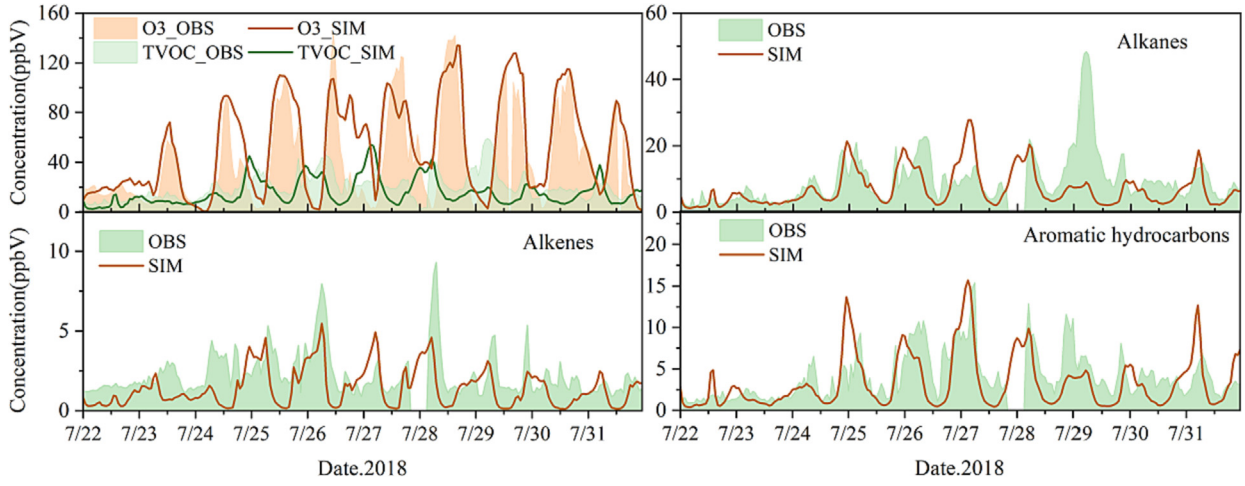

Fig. 2. Comparisons of hourly observations and simulated concentrations of VOCs species and O_3 at Dianshan Lake supersite.

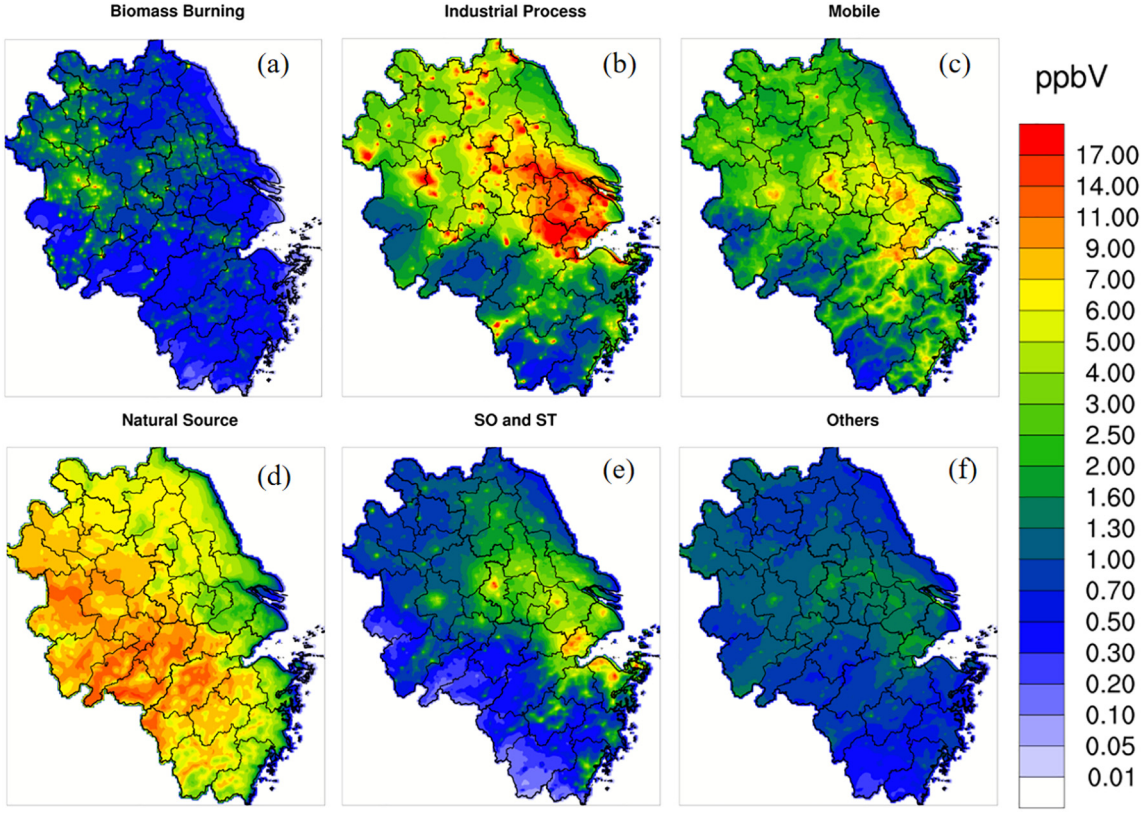

Fig. 3. Spatial distribution of average contributions of each VOC emission source from July 13 to 31, 2018. SO represents solvent usage, and ST represents oil and gas storage and transportation. Others represents the sources including residential combustion, power plants, industrial boilers and kilns, and waste treatment.

isoprene during transport from other regions; therefore, the contribution of natural sources based on the PMF method is highly underestimated. For example, the contribution from natural source emissions in the ISAM results was 14.7 %, whereas its contribution based on the PMF method was only 6.1 % (Fig. 5). Likewise, in Table S11, the contributions from biogenic emission based on the ISAM were much higher than those of PMF, except for the

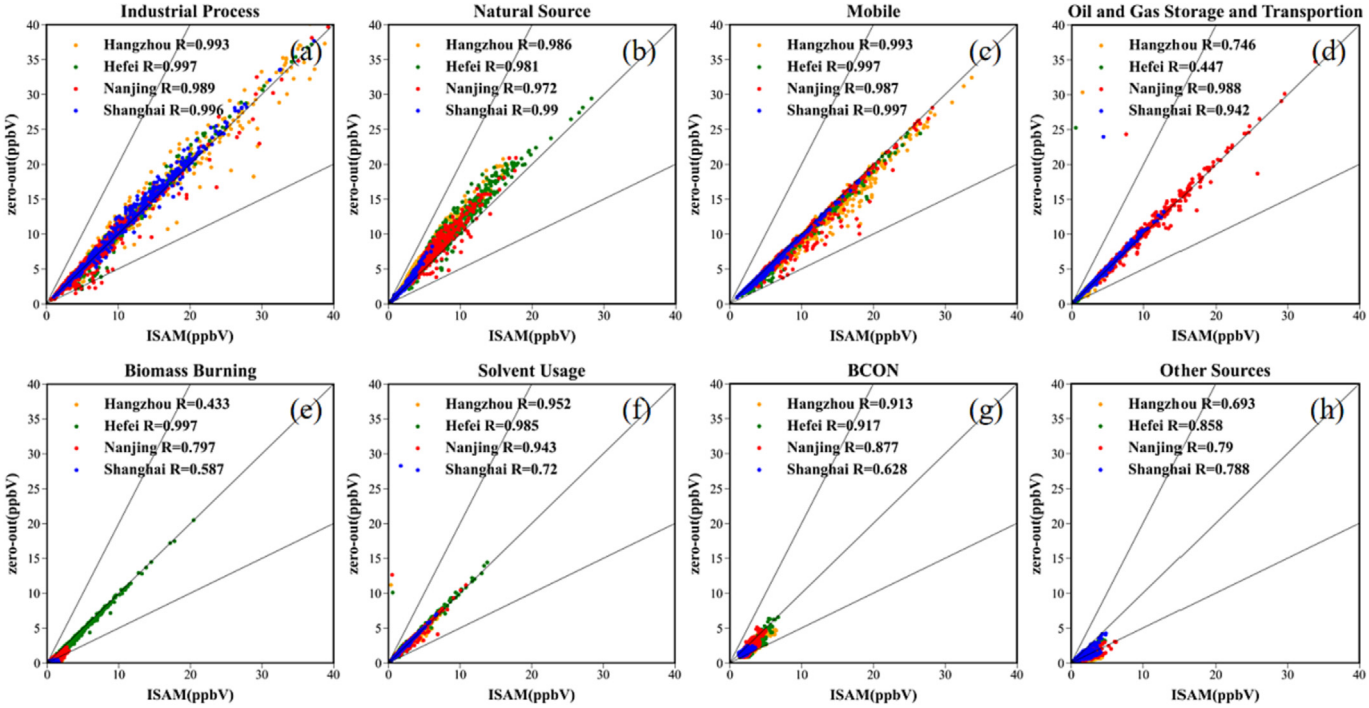

Fig. 4. Comparisons of source contributions to VOCs concentrations based on ISAM/zero-out for each sector and all simulated hours. Orange: Hangzhou; Green: Hefei; Red: Nanjing; Blue: Shanghai; BCON: transport contribution from emissions outside the simulation area. Other sources include Waste treatment, Power plants, Industrial boilers and kilns, and Residential combustion.

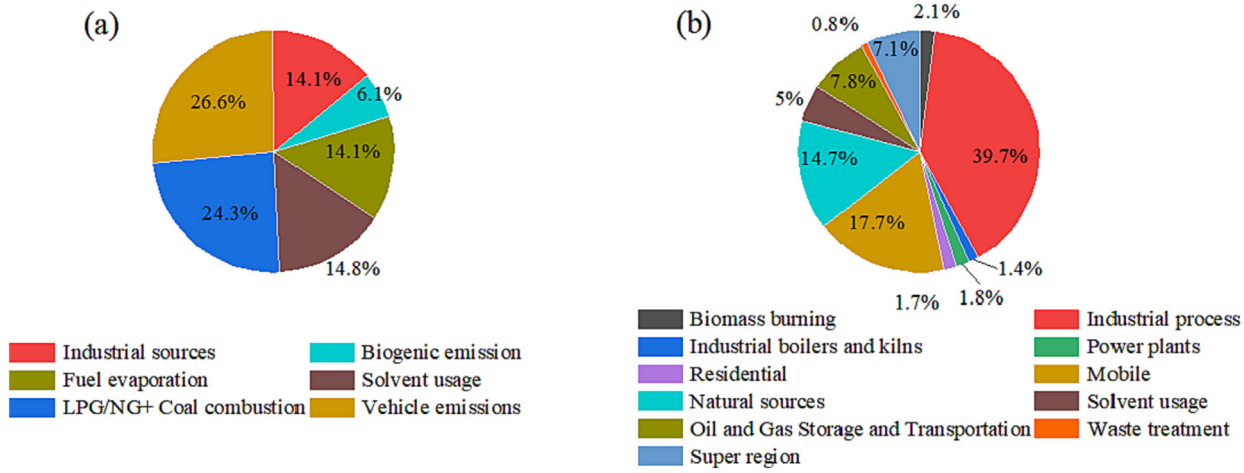

Fig. 5. Comparison of the PMF (a) and the ISAM (b) results of Dianshan Lake supersite during July. 24–31, 2018.

receptor of the Huapu site which is in the West Lake viewing area surrounded by a lot of plants. In addition, the contribution to the Dianshan Lake supersite from vehicle sources based on the PMF method was overestimated. In contrast, the contribution from industrial processes was underestimated using the PMF method. Furthermore, the contribution of long-distance transport was resolved to be 6.4 % by the ISAM, whereas the PMF method could not identify any regional contribution.

Vegetation emits VOCs species, such as isoprene and terpenes, but these emitted compounds can produce aromatics through chemical reactions in the atmosphere. The ISAM integrates these chemical processes and can resolve a specific contribution to atmospheric aromatics from natural sources, although the contribution is small (Fig. 6), which cannot be achieved by PMF. Fig. 6 also shows that the contribution of natural sources in southern Zhejiang, and western and south Anhui to atmospheric aromatics was relatively high owing to rich vegetation. Theoretically, the ISAM integrates the comprehensive processes of emissions, meteorology, and chemistry, so that it not only resolves the source contributions of geographic regions but also considers the effects of chemical reactions and losses.

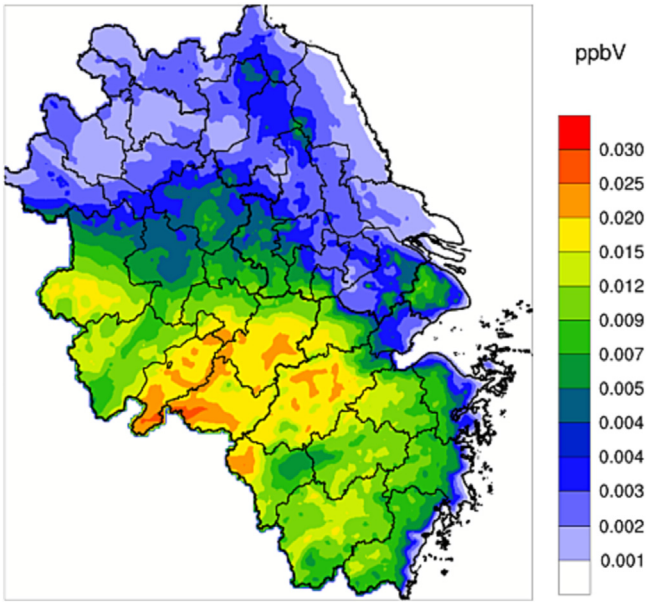

Fig. 6. Contribution from natural sources to aromatic hydrocarbons over the YRD region.

3.5. Regional contributions of O_3, VOC and NO_x

During the period of July 24–30, one heavily polluted episode of O_3, with the maximum concentration exceeding 200 μg/m^3 (Fig. S2), occurred over the YRD region following a typhoon (Typhoon Ampil) that landed near Shanghai city on 22 July (wang et al., 2022a). The contribution percentages of regional sources of O_3, VOCs, and NO_x during the pre-typhoon clean period (July 13–20) and post-typhoon ozone polluted period (July 24–30) in the four provincial capital cities in the summer of 2018 are shown in Fig. 7. The percentage of contribution from local city to O_3, VOCs, and NO_x at urban sites is all greater than those of suburban sites for these provincial capital cities, probably because, on the one hand, there are fewer high-rise buildings in the suburbs than in the urban, which facilitates the transport of pollutants. On the other hand, most of the emission sources are concentrated in urban areas. Shanghai Dianshan Lake super site is an exception, during the polluted period, 33 % of the VOCs came from Zhejiang province, 16 % from Jiangsu province, and only 20 % from Shanghai, mainly because it is close to the borders of Zhejiang and Jiangsu. In these four cities, the local contribution percentages of O_3 ranged from 15 % to 33 %, which were generally lower than the super-regional contribution percentages, which ranged from 30 % to 60 % whether urban or suburban receptor sites, suggesting that regional transport plays a crucial role in the formation of O_3 over the YRD region. Because the southerly wind was dominant throughout the clean period (Fig. S7a), super-regional transport was the largest contributor to O_3 in Shanghai and Hangzhou, with contribution percentages of 53 %–60 %, and their second largest contributor was Zhejiang (14 %–30 %). During the clean period, the largest contributor to O_3 in Nanjing and Hefei was super-regional transport (38 %–46 %), followed by Zhejiang (22 %–28 %), and the local contributions only ranged from 16 % to 21 %. During the polluted period, the southwest wind was dominant; however, on the border of the three provinces and one city, the air mass shifted southward and northward. (Fig. S7c). Jiangsu, Zhejiang, and Anhui provinces and Shanghai contributed significantly to ozone in these capital cities.

Compared with the polluted period, the super-regional contribution percentage of O_3 was larger. In contrast, the contribution percentages from local and its surrounding areas were slightly lower during the clean period. Regions (non-local) that contributed a lot to O_3 also contributed a lot to NO_x at the same receptor site, and their contribution percentages are very close. In both the clean and polluted periods, the local contributions of NO_x at the urban sites ranged from 31 % to 43 %, and those at the suburban sites ranged from 25 % to 30 %, both higher than O_3. However, the local contribution percentages of VOCs at the urban sites ranged from 60 % to 77 %, far higher than those of NO_x and O_3.

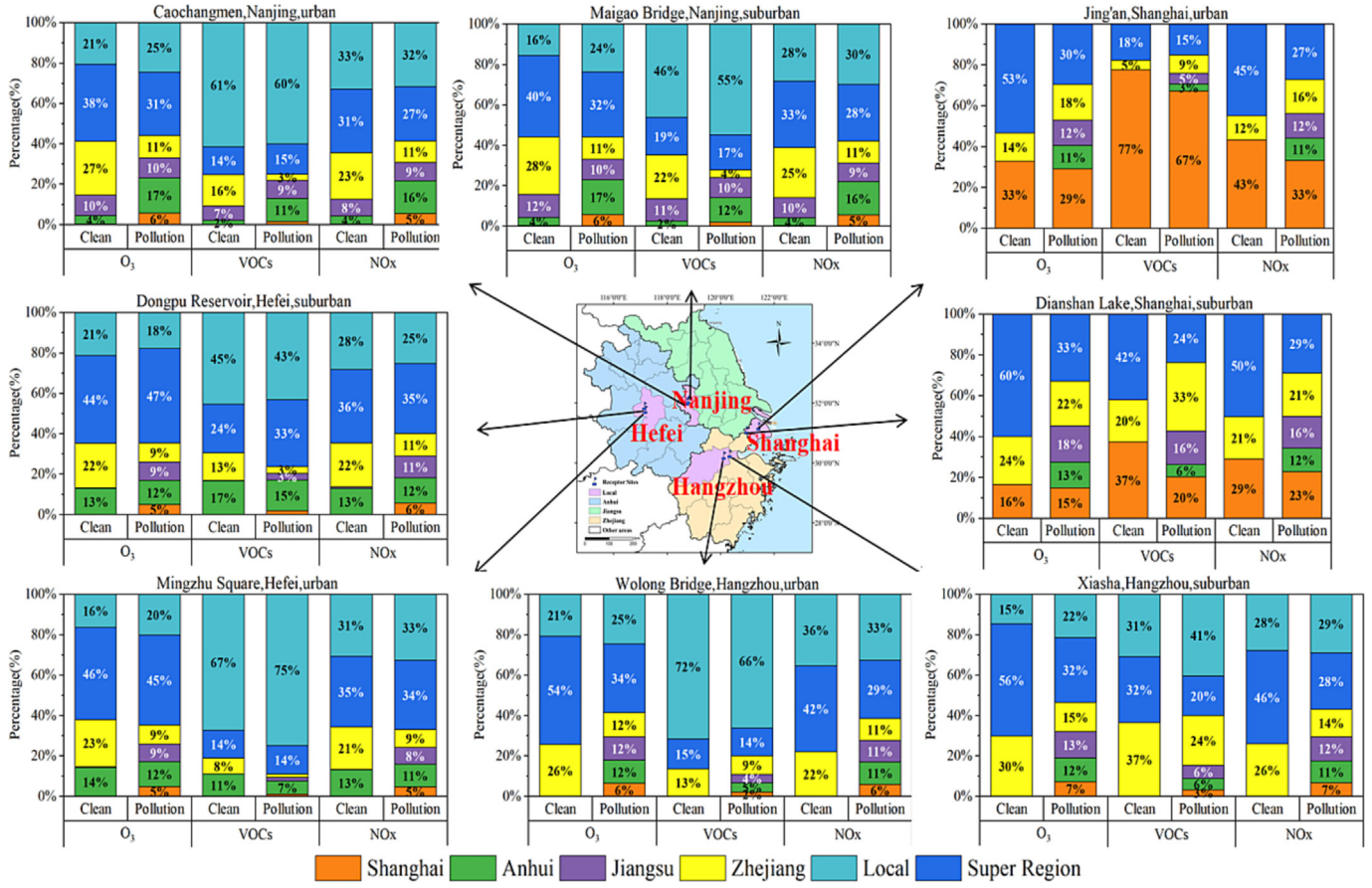

Fig. 7. Averaged regional contributions to O_3, NO_x, and VOCs for each day from 9:00 to 16:00 during clean (July 13 -20) and polluted (July 24–30) periods, respectively. The contribution from Zhejiang province to any pollutants at the sites of Hangzhou did not include the contribution from Hangzhou, which belongs to the local contribution. Likewise, Jiangsu Province's contribution to Nanjing and Anhui Province's contribution to Hefei also did not include the contributions from their local cities (Nanjing/Hefei). The contribution from Shanghai to any pollutants at the sites of Shanghai is local. The super region's contribution represents the contribution from outside the YRD region.

Generally, the regional contribution patterns of O_3 are similar to those of NO_x, both of which have strong abilities of long-distance transport. However, they are very different from VOCs, mainly because VOCs experience a large amount of chemical loss during the transport process, and NO_x (NO and NO_2) and O_3 undergo mutual conversion and circulation during the transport process. Thus, their chemical loss is much smaller than that of VOCs.

3.6. Difference in transport contributions of NO_x, VOCs, and O_3

Fig. S8 shows the regional hourly contribution concentrations to O_3 of urban and suburban sites of the four provincial capital cities from July 13–31, 2018. From the early morning of July 24 at Caochangmen Station in Nanjing, the transport contributions from Shanghai, Anhui, Jiangsu (excluding Nanjing) and Zhejiang provinces to Nanjing's NO_x began to increase and accumulate. The contribution from these regions to Nanjing's O_3 during the daytime of the polluted period increased with a similar contribution percentage of these region to Nanjing's NO_x on the last night. Notably, the contributions from Shanghai and Zhejiang provinces to Nanjing's VOC are almost negligible, but the contributions of these regions to O_3 are still large. Moreover, the average wind speed in Nanjing during this polluted period was moderate (1.86 m/s, Table S12), making NO_x and O_3 have a strong transport capability. Therefore, the contribution from Shanghai and Zhejiang to Nanjing's O_3 is a main result of the transport contribution of O_3 itself and the chemical contribution from NO_2 during the transport of NO_x, which was mainly composed of NO_2 within the aged air mass, rather than the chemical contribution of VOCs during transport to Nanjing's O_3. Shanghai, Hefei, and Hangzhou also had similar contribution patterns to Nanjing (Fig. S8). From the perspective of the entire YRD region (Fig. S9), the regional contributions of NO_x, VOCs and O_3 are obviously different. O_3 and NO_x were more easily transported to farther places than VOCs. During medium- and long-distance transport, NO_2 photolysis at wavelengths of sunlight <424 nm produced oxygen atoms, which then quickly combined with O_2 to generate O_3 ($O + O_2 + M \rightarrow O_3 + M$). This chemical process promoted an increase in the amount of O_3 during the transport process, resulting in a similar percentage of contributions from medium- and long-distance transport to NO_x and O_3. This information is essential in understanding the influence of medium- and long-distance transport on O_3 formation in urban agglomeration areas with many human activities, especially during O_3 polluted episodes.

As shown in Fig. 8, NO_x's regional transport contribution percentages were significantly more correlated with the same region's contribution percentages of O_3 than those of their local contributions. For example, Hangzhou was the receptor site during the polluted period. The contribution percentages from super-region transport, Zhejiang (excluding Hangzhou), Jiangsu, Anhui, and Shanghai all had strong correlations of 0.91, 0.98, 0.98, 0.97, and 0.99 between NO_x and O_3, respectively, which were far higher than that of local (0.59), mainly because NO_x, mainly NO_2 in highly aged air masses, generated oxygen atoms through photolysis and then promoted the generation of O_3 during the transport processes of O_3 and NO_x. By contrast, NO_x contributed locally contained a high proportion of NO due to fresher air masses. These NO reacted with O_3, resulting in a decrease of O_3 concentration to a certain extent, leading to a relatively weak correlation of local contribution percentages between NO_x and O_3 compared with the medium- and long-distance contributions. Nanjing and Hangzhou also had the same pattern for the NO_x and O_3 correlation (Fig. 8). Nevertheless,

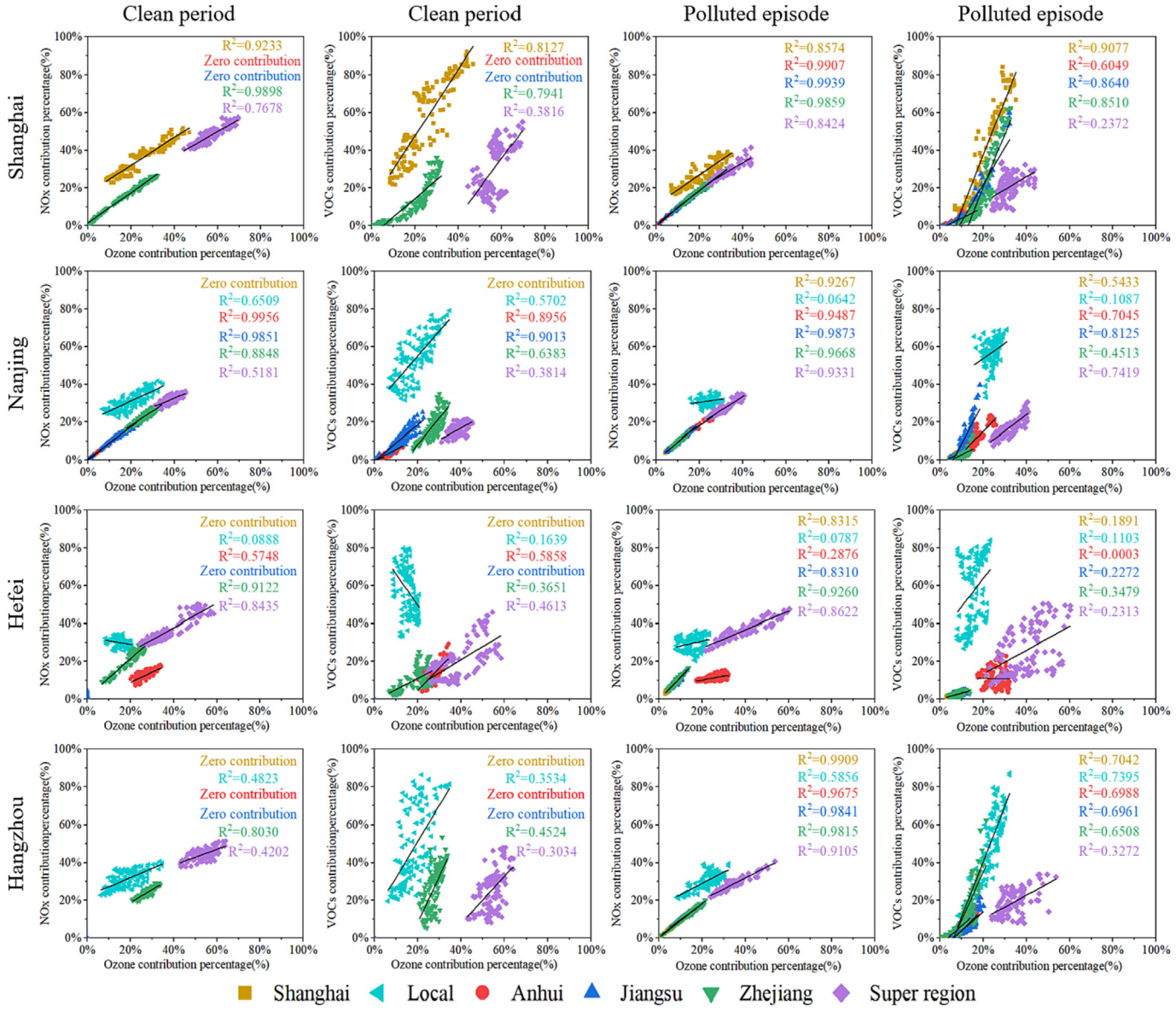

Fig. 8. The correlation between the contribution percentages of O_3 and its precursors (VOC and NO_x) for different cities (both sites included) during the clean and polluted periods from 9:00 to 16:00, respectively. The contribution from Zhejiang province to any pollutant in the sites of Hangzhou did not include the contribution from Hangzhou, which belongs to the local contribution. Likewise, Jiangsu Province's contribution to Nanjing and Anhui Province's contribution to Hefei also did not include the contribution from their local city (Nanjing/Hefei). The contribution from Shanghai to any pollutant in the sites of Shanghai is local. The super region's contribution represents the contribution from outside the YRD region.

Shanghai and Hangzhou were somewhat different from this. Shanghai is an international metropolis with a large city area; thus, the local contribution of Shanghai also includes partial longer-distance transport contributions, although they are from regions within Shanghai. The correlation between the local contribution percentages of NO_x and O_3 in Shanghai (0.86) was higher than that in Hangzhou (0.59). As for Hefei, the receptor site (Hefei) is relatively close to Anhui (non-Hefei), especially the sources of high NO_x emissions in Anhui (non-Hefei), such as Maanshan Iron and Steel, etc. are close to Hefei, and the transport distance is relatively short, leading to a low correlation (0.29) of NO_x and O_3 from Anhui (non-Hefei). For the clean period, the aging degree of air masses from the southeast was lower than that of the polluted period from continental areas. Therefore, the correlations of contribution percentages between NO_x and O_3 of these cities from medium-distance and long-distance contributions were also relatively low.

Compared with NO_x, the regional transport contribution percentage of VOCs was generally less correlated with O_3, mainly because of the chemical loss of VOCs caused by the reaction of OH radicals and the chemical cycle between NO_x and O_3 during their regional transport. In addition, the low local contribution percentages of O_3 (15 %–33 %) and the perturbation effect of NO in local fresh air masses on O_3 are likely to lead to a weak correlation between the local contribution percentages of VOCs and O_3, although VOCs have a positive effect on O_3 production in terms of chemical mechanisms.

In general, the regional contributions of NO_x and O_3 are highly correlated, and the regional transport of NO_x has a significant impact on the formation of O_3, especially during the period of O_3 heavy pollution; the regional transport of NO_x has a greater effect on O_3, suggesting that O_3 is more sensitive to NO_x in the polluted period, which is consistent with another study (Wang et al., 2022a). In that study, a sensitivity analysis of O_3 in the YRD region was conducted based on the higher-order decoupled direct method tools embedded in the Community Multiscale Air Quality model (CMAQ-HDDM) on July 24–31, 2018, and the results showed that the first-order sensitivity of O_3 to NO_x increased sharply from 10:00 am

and reached its peak at approximately 14:00. Therefore, it is concluded that reducing NO_x concentration in regional transport is probably an important measure to reduce the O_3 concentration in these cities. In other words, strengthening the joint prevention and control of NO_x emissions between regions or cities is a critical way to reduce regional O_3 concentration during such kind of O_3 polluted episodes.

4. Conclusions

In this study, the source apportionment of VOCs, NO_x, and O_3 over the YRD region during the O_3 polluted episode in July 2018 was performed simultaneously based on the CMAQ-ISAM model, and the differences between the transport contributions of VOCs and NO_x and their impacts on O_3 were investigated. The result of model performance evaluation indicates that the IOA values of alkanes, aromatic hydrocarbons, alkenes, and TVOC were 0.55, 0.74, 0.62 and 0.67, respectively. Generally, the observations of VOCs species were well captured by the simulations.

The source apportionment results of the BFM generally correlated well with those based on the ISAM, but the contribution percentages of natural sources to VOCs resulting from the BFM were slightly higher, because of the slight deviations of the BFM in quantitatively identifying sources emitting pollutants with high chemical reactivity. In addition, the PMF was less able to quantitatively identify the contribution from sources emitting highly reactive VOCs species because the PMF model identifies a contributing factor as a specific source based on its similarity to the emission profile of this specific source. Consequently, the PMF prefers to apportion low-reactivity VOCs to their source. In summary, the ISAM is more advanced and accurate than either BFM or PMF for source apportionment of VOCs, as well as NO_x and O_3, because the ISAM not only absorbs the information on the emission inventory and meteorological field, but also integrates the physical transport mechanism and relatively complete chemical mechanism.

In the clean and polluted periods, the local contribution percentages of VOCs in urban sites of four provincial capital cities ranged from 60 % to 77 %, much higher than those of NO_x (31 %–43 %) and O_3 (16 %–33 %). Both NO_x and O_3 have strong transport abilities, with high and close contribution percentages, which are highly correlated. This is because during medium- and long-distance transport, NO_x is mainly composed of NO_2 due to the influence of high aging air mass, subsequently, the oxygen atoms produced by the photolysis of NO_2 quickly combine with O_2 to form O_3 during transport, forming a symbiotic relationship between NO_x and O_3 during transport. This suggests that the regional transport of NO_x potentially enhances the regional transport of O_3. For VOCs, the chemical loss caused by the oxidation of OH radicals during transport makes the contribution of VOCs from long-distance transport much smaller than that of NO_x. Furthermore, owing to the sufficient aging of VOCs, the VOCs from long-distance transport contributed little to O_3. As a result, chemical loss makes the long-distance transport contribution of VOCs less correlated with O_3.

Controlling VOCs emissions in local city and NO_x emissions in its upwind cities is of great significance to mitigate O_3 pollution in a specific city. To strengthen the mutual benefits among cities, the joint control of NO_x among cities, even long-distance regions, is critical to alleviate O_3 pollution, thereby reducing the overall concentration of O_3 in a larger-scale region. To a certain extent, controlling one's NO_x emissions can help other cities more, while controlling one's VOCs emissions can help itself more. It is recommended to pay enough attention to joint prevention and control of NO_x among surrounding cities and even long-distance areas to alleviate regional O_3 pollution.

CRediT authorship contribution statement

Yangjun Wang: Conceptualization, Methodology, Software, Visualization, Validation, Data curation, Writing-original draft preparation, Funding Acquisition.

Li Li: Conceptualization, Methodology, Funding Acquisition.

Sen Jiang: Methodology, Software, Visualization, Validation, Data curation, Writing-original draft preparation

Ling Huang: Software, Visualization

Manomaiphiboon Kasemsan: Methodology

Guibin Lu, Jiaqiang Liao, Hanqing Liu and Jinting Bian: Software

Elly Arukulem Yaluk: Software, Visualization

Kun Zhang and Hui Chen: Writing-reviewing and editing.

Data availability

Data will be made available on request.

Declaration of competing interest

The authors declare that they have no conflict of interest.

Acknowledgement

This study was financially supported by Open Foundation of State Environmental Protection Key Laboratory of Sources and Control of Air Pollution Complex (NO. SCAPC202003), the National Natural Science Foundation of China (NOS. 42075144, 42005112), and the Shanghai International Science and Technology Cooperation Fund (NO. 19230742500). We also appreciate the High-Performance Computing Center of Shanghai University and Shanghai Engineering Research Center of Intelligent Computing System (NO. DZ2252600) for providing the computing resources and technical support. We are grateful for the anonymous comments of for the anonymous comments of reviewers.

Appendix A. Supplementary data

Supplementary data to this article can be found online at https://doi.org/10.1016/j.scitotenv.2023.162118.

References

Adam, R., 2007. Receptor modeling of ambient particulate matter data using positive matrix factorization: review of existing methods. Journal of the Air & Waste Management Association 57 (2), 146–154.

Badol, C., Locoge, N., Galloo, J.C., 2008. Using a source-receptor approach to characterise VOC behaviour in a french urban area influenced by industrial emissions - part II: source contribution assessment using the chemical mass balance (CMB) model. Sci. Total Environ. 389 (2–3), 429–440.

Carter, W.J.A.E., 2010. Development of the SAPRC-07 chemical mechanism. 44 (40), 5324–5335.

Cohen, A.J., Brauer, M., Burnett, R., Anderson, H.R., Frostad, J., Estep, K., Balakrishnan, K., Brunekreef, B., Dandona, L., Dandona, R., Feigin, V., Freedman, G., Hubbell, B., Jobling, A., Kan, H., Knibbs, L., Liu, Y., Martin, R., Morawska, L., Pope, C.A., Shin, H., Straif, K., Shaddick, G., Thomas, M., van Dingenen, R., van Donkelaar, A., Vos, T., Murray, C.J.L., Forouzanfar, M.H., 2017. Estimates and 25-year trends of the global burden of disease attributable to ambient air pollution: an analysis of data from the global burden of diseases study 2015. Lancet 389 (10082), 1907–1918.

Craig, K., Erdakos, G., Chang, S.Y., Baringer, L., 2020. Air quality and source apportionment modeling of year 2017 ozone episodes in Albuquerque/Bernalillo County, New Mexico. J. Air Waste Manage. Assoc. 70 (11), 1101–1120.

Fan, M.-Y., Zhang, Y.-L., Lin, Y.-C., Li, L., Xie, F., Hu, J., Mozaffar, A., Cao, F., 2021. Source apportionments of atmospheric volatile organic compounds in Nanjing, China during high ozone pollution season. Chemosphere 263.

Fang, T., Zhu, Y., Jang, J., Wang, S., Xing, J., Chiang, P.C., Fan, S., You, Z., Li, J., 2020. Real-time source contribution analysis of ambient ozone using an enhanced meta-modeling approach over the Pearl River Delta region of China. J. Environ. Manag. 268, 110650.

Hu, Y.T., Odman, M.T., Russell, A.G., Kumar, N., Knipping, E., 2022. Source apportionment of ozone and fine particulate matter in the United States for 2016 and 2028. Atmos. Environ. 285.

Kang, M.J., Hu, J.L., Zhang, H.L., Ying, Q., 2022. Evaluation of a highly condensed SAPRC chemical mechanism and two emission inventories for ozone source apportionment and emission control strategy assessments in China. Sci. Total Environ. 813.

Koo, B., Wilson, G.M., Morris, R.E., Dunker, A.M., Yarwood, G., 2009. Comparison of source apportionment and sensitivity analysis in a particulate matter air quality model. Environ. Sci. Technol. 43 (17), 6669–6675.

Kwok, R.H.F., Baker, K.R., Napelenok, S.L., Tonnesen, G.S., 2015. Photochemical grid model implementation and application of VOC, NOx, and O-3 source apportionment. Geosci. Model Dev. 8 (1), 99–114.

Li, X.B., Fan, G.Q., 2022. Interannual variations, sources, and health impacts of the springtime ozone in Shanghai. Environ. Pollut. 306.
Li, S., Harley, P.C., Niinemets, U., 2017. Ozone-induced foliar damage and release of stress volatiles is highly dependent on stomatal openness and priming by low-level ozone exposure in Phaseolus vulgaris. Plant Cell Environ. 40 (9), 1984–2003.
Li, J.F., Wang, Y.H., Qu, H., 2019a. Dependence of summertime surface ozone on NOx and VOC emissions over the United States: peak time and value. Geophys. Res. Lett. 46 (6), 3540–3550.
Li, L., An, J., Huang, L., Yan, R., Huang, C., Yarwood, G., 2019b. Ozone source apportionment over the Yangtze River Delta region, China: investigation of regional transport, sectoral contributions and seasonal differences. Atmos. Environ. 202, 269–280.
Lin, Y.H., Zhang, H., Pye, H.O., Zhang, Z., Marth, W.J., Park, S., Arashiro, M., Cui, T., Budisulistiorini, S.H., Sexton, K.G., Vizuete, W., Xie, Y., Luecken, D.J., Piletic, I.R., Edney, E.O., Bartolotti, L.J., Gold, A., Surratt, J.D., 2013. Epoxide as a precursor to secondary organic aerosol formation from isoprene photooxidation in the presence of nitrogen oxides. Proc. Natl. Acad. Sci. U. S. A. 110 (17), 6718–6723.
Lu, X., Yao, T., Li, Y., Fung, J.C.H., Lau, A.K.H., 2016. Source apportionment and health effect of NOx over the Pearl River Delta region in southern China. Environ. Pollut. 212, 135–146.
Lupascu, A., Otero, N., Minkos, A., Butler, T., 2022. Attribution of surface ozone to NOx and volatile organic compound sources during two different high ozone events. Atmos. Chem. Phys. 22 (17), 11675–11699.
Monks, P.S., Archibald, A.T., Colette, A., Cooper, O., Coyle, M., Derwent, R., Fowler, D., Granier, C., Law, K.S., Mills, G.E., Stevenson, D.S., Tarasova, O., Thouret, V., von Schneidemesser, E., Sommariva, R., Wild, O., Williams, M.L., 2015. Tropospheric ozone and its precursors from the urban to the global scale from air quality to short-lived climate forcer. Atmos. Chem. Phys. 15 (15), 8889–8973.
Murphy, B.N., Woody, M.C., Jimenez, J.L., Carlton, A.M.G., Hayes, P.L., Liu, S., Ng, N.L., Russell, L.M., Setyan, A., Xu, L., Young, J., Zaveri, R.A., Zhang, Q., Pye, H.O.T., 2017. Semivolatile POA and parameterized total combustion SOA in CMAQv5.2: impacts on source strength and partitioning. Atmos. Chem. Phys. 17, 11107–11133.
Norris, G., Duvall, R., Brown, S., Bai, S., 2014. EPA Positive Matrix Factorization (PMF) 5.0 Fundamentals and User Guide.
Pye, H.O., Luecken, D.J., Xu, L., Boyd, C.M., Ng, N.L., Baker, K.R., Ayres, B.R., Bash, J.O., Baumann, K., Carter, W.P., Edgerton, E., Fry, J.L., Hutzell, W.T., Schwede, D.B., Shepson, P.B., 2015. Modeling the current and future roles of particulate organic nitrates in the southeastern United States. Environ. Sci. Technol. 49 (24), 14195–14203.
Ren, J., Guo, F.F., Xie, S.D., 2022. Diagnosing ozone-NOx-VOC sensitivity and revealing causes of ozoneincreases in China based on 2013–2021 satellite retrievals. Atmos. Chem. Phys. 22 (22), 15035–15047.
Shao, M., Wang, B., Lu, S.H., Yuan, B., Wang, M., 2011. Effects of Beijing olympics control measures on reducing reactive hydrocarbon species. Environ. Sci. Technol. 45 (2), 514–519.
Shu, L., Wang, T., Xie, M., Li, M., Zhao, M., Zhang, M., Zhao, X., 2019. Episode study of fine particle and ozone during the CAPUM-YRD over Yangtze River Delta of China: characteristics and source attribution. Atmos. Environ. 203, 87–101.
Sillman, S., 1999. The relation between ozone, NOx and hydrocarbons in urban and polluted rural environments. Atmos. Environ. 33 (12), 1821–1845.
Su, Y.C., Chen, W.H., Fan, C.L., Tong, Y.H., Weng, T.H., Chen, S.P., Kuo, C.P., Wang, J.L., Chang, J.S., 2019. Source apportionment of volatile organic compounds (VOCs) by positive matrix factorization (PMF) supported by model simulation and source markers - using petrochemical emissions as a showcase. Environ. Pollut. 254.
Turner, M.C., Jerrett, M., Pope, C.A., Krewski, D., Gapstur, S.M., Diver, W.R., Beckerman, B.S., Marshall, J.D., Su, J., Crouse, D.L., Burnett, R.T., 2016. Long-term ozone exposure and mortality in a large prospective study. Am. J. Respir. Crit. Care Med. 193 (10), 1134–1142.
Vestenius, M., Hopke, P.K., Lehtipalo, K., Petaja, T., Hakola, H., Hellen, H., 2021. Assessing volatile organic compound sources in a boreal forest using positive matrix factorization (PMF). Atmos. Environ. 259.
Wagstrom, K.M., Pandis, S.N., Yarwood, G., Wilson, G.M., Morris, R.E., 2008. Development and application of a computationally efficient particulate matter apportionment algorithm in a three-dimensional chemical transport model. Atmos. Environ. 42 (22), 5650–5659.
Wang, H.K., Huang, C.H., Chen, K.S., Peng, Y.P., Lai, C.H., 2010. Measurement and source characteristics of carbonyl compounds in the atmosphere in Kaohsiung CityTaiwan. Journal of Hazardous Materials 179 (1–3), 1115–1121.
Wang, X.L., Fu, T.M., Zhang, L., Cao, H.S., Zhang, Q., Ma, H.C., Shen, L., Evans, M.J., Ivatt, P.D., Lu, X., Chen, Y.F., Zhang, L.J., Feng, X., Yang, X., Zhu, L., Henze, D.K., 2021a. Sensitivities of ozone air pollution in the Beijing-Tianjin-Hebei area to local and upwind precursor emissions using adjoint modeling. Environmental Science & Technology 55 (9), 5752–5762.
Wang, Y.J., Tan, X.J., Huang, L., Wang, Q., Li, H.L., Zhang, H.Y., Zhang, K., Liu, Z.Y., Traore, D., Yaluk, E., Fu, J.S., Li, L., 2021b. The impact of biogenic emissions on ozone formation in the Yangtze River Delta region based on MEGANv3.1. Air Qual. Atmos. Health 14 (5), 763–774.
Wang, Y.J., Yaluk, E.A., Chen, H., Jiang, S., Huang, L., Zhu, A.S., Xiao, S.L., Xue, J., Lu, G.B., Bian, J.T., Kasemsan, M., Zhang, K., Liu, H.Q., Tong, H.H., Ooi, M.C.G., Chan, A., Li, L., 2022a. The importance of NOx control for peak ozone mitigation based on a sensitivity study using CMAQ-HDDM-3D model during a typical episode over the Yangtze River Delta regionChina. Journal of Geophysical Research-Atmospheres 127 (19).
Wang, Z., Shi, Z., Wang, F., Liang, W., Shi, G., Wang, W., Chen, D., Liang, D., Feng, Y., Russell, A.G., 2022b. Implications for ozone control by understanding the survivor bias in observed ozone-volatile organic compounds system. Npj climate and atmospheric. Science 5 (1).
Xing, J., Wang, S., Zhao, B., Wu, W., Ding, D., Jang, C., Zhu, Y., Chang, X., Wang, J., Zhang, F., Hao, J., 2017. Quantifying nonlinear multiregional contributions to ozone and fine particles using an updated response surface modeling technique. Environ Sci Technol 51 (20), 11788–11798.
Yang, M.R., Li, F.X., Huang, C.Y., Tong, L., Dai, X.R., Xiao, H., 2023. VOC characteristics and their source apportionment in a coastal industrial area in the Yangtze River Delta, China. J. Environ. Sci. 127, 483–494.
Yuan, B., Shao, M., de Gouw, J., Parrish, D.D., Lu, S.H., Wang, M., Zeng, L.M., Zhang, Q., Song, Y., Zhang, J.B., Hu, M., 2012. Volatile organic compounds (VOCs) in urban air: how chemistry affects the interpretation of positive matrix factorization (PMF) analysis. J. Geophys. Res.-Atmos. 117.